Title
POTENTIAL IMPROVEMENTS IN INSTRUMENTATION FOR PET

Author
Derenzo, S.E.

Publication Date
1984-09-01

Lawrence Berkeley Laboratory
UNIVERSITY OF CALIFORNIA

Presented at the NATO Advanced Studies Institute Series - Physics and Engineering of Medical Imaging, Maratea, Italy, September 23 - October 5, 1984

POTENTIAL IMPROVEMENTS IN INSTRUMENTATION FOR PET

S.E. Derenzo

September 1984

Donner Laboratory

Biology & Medicine Division

Prepared for the U.S. Department of Energy under Contract DE-AC03-76SF00098

DISCLAIMER

POTENTIAL IMPROVEMENTS IN INSTRUMENTATION FOR PET

Stephen E. Derenzo

Lawrence Berkeley Laboratory
and Donner Laboratory
University of California
Berkeley, CA 94720
U.S.A.

ABSTRACT

This paper discusses the potential for improved detectors in Positron Emission Tomography (PET) and explores the ultimate limits that might be achieved in the areas of spatial resolution, sensitivity, and maximum imaging rates. It is shown that if an ultra-fast, high efficiency scintillator and a thin, low-noise, position-sensitive photodetector were available, a multi-layer time-of-flight tomograph would be possible with a 10 cm axial field of view, a 3-dimensional spatial resolution of 2 mm fwhm, and >700,000 prompt unscattered coincidences per sec for 1 μCi per cm^3 in a 20 cm diam cylinder of water.

1 IMPROVED DETECTORS

1.1 SCINTILLATION CRYSTALS

Table 1 lists properties of three detector materials commonly used in positron tomographs, NaI(Tl), BaF_2, and bismuth germanate (BGO). NaI(Tl) has the best photon yield and pulse height resolution, BaF_2 has the best timing resolution, and BGO has the best detection efficiency. An "ideal detector" with the best properties of all three has not yet been found. However, the scintillation properties of three important heavy inorganic crystals have been discovered rather recently: BaF_2 in 1971 (1), BGO in 1973 (2), the fast component of BaF_2 in 1982 (3,4), and GSO in 1982 (5). Further efforts in this direction are essential if the potentials of PET are to be fully realized.

TABLE 1. PROPERTIES OF SCINTILLATION MATERIALS FOR POSITRON EMISSION TOMOGRAPHY

Material	NaI(Tl)	BaF_2	BGO	"Ideal Detector"
Density (gm/cm^3)	3.67	4.8	7.13	>7
Atomic numbers	11,53	56,9	83,32,8	>80
Index of refraction	1.85	1.56	2.15	$\simeq 2^a$
Hygroscopic?	YES	NO	NO	NO
Photoelectron yield (511 keV)	2,500	800;200	300	>1,000[b]
Scintillation decay time (nsec)	230	620;0.8	300	<1
Photoelectrons/nsec (peak rate)	11	1.3;250	1	>1,000
Time resolution (fwhm nsec)	1.5	0.2	5	<0.2
Energy resolution (% fwhm)	7	20	10	<8
INTERACTION PROBABILITIES FOR 511 keV PHOTONS:				
Photoelectric (cm^{-1})	0.060	0.085	0.393	>0.4
Compton (cm^{-1})	0.268	0.353	0.510	>0.5
Total (cm^{-1})	0.328	0.438	0.903	>0.9
Photoelectric fraction[c]	0.183	0.194	0.435	>0.4

[a]A high index is chosen to define a photon "escape cone" that can be used to determine the position of interaction in 3 dimensions (see section 2.1 below).
[b]Efficient coupling to a phototube (20% quantum efficiency) or escape cone coupling to a solid state photodetector (80% quantum efficiency)
[c]Ratio of photoelectric/total, or the probability of full photoelectric absorption on the first interaction

1.2 SOLID STATE DETECTORS

While germanium detectors have been suggested for the detection of annihilation photons in positron emission tomography (6,7), it is not possible to use their excellent pulse height resolution because their photopeak detection efficiency is extremely low. For example, there is only a 5% probability that an incident 511 keV photon will deposit all its energy in a 5 mm x 5 mm x 30 mm deep germanium crystal (8). The detection efficiency can be significantly improved (to over 50%) by using a low pulse height threshold, but the efficiency is still well below that of the heavy element scintillators. Both HgI_2 and CdTe have good detection efficiency due to their high atomic numbers and densities but have not yet been developed to the point where thousands of detectors can be used in large tomographs. The development of such heavy element semiconductors (9,10), would provide an attractive alternative to the scintillator detector by eliminating the photomultiplier coupling problem and by providing better pulse height resolution than scintillation detectors.

1.3 COMBINED PHOTOTUBE- SOLID STATE READOUT

One promising approach uses a photomultiplier combined with solid state photodetectors. A group of crystals is coupled to a relatively large photomultiplier tube which determines the timing for the group. The solid-state photodetectors are coupled individually to each crystal to determine the identity of the scintillating crystal. HgI_2 (11-13), silicon photodiodes (14-16), silicon avalanche photodiodes (17-20), and small low-gain phototubes (21) have been suggested for the crystal identifier. This method is good for very small crystals, since the noise of solid state photodetectors decreases with decreasing area, and the signal is nearly independent of crystal size. In addition, it permits the rejection of multiple-crystal interactions that degrade spatial resolution.

This approach has been demonstrated using a 3 mm wide BGO crystal in coincidence with two 3 mm wide BGO crystals coupled to a common 14 mm PMT and individually coupled to silicon photodiodes. The signal to noise ratio was adequate for the identification of the individual crystals on an event-by-event basis and the measured detector pair resolution was 2.0 mm fwhm (14,15). A multi-layer positron tomograph design using this technology is sketched in Figures 1 and 2.

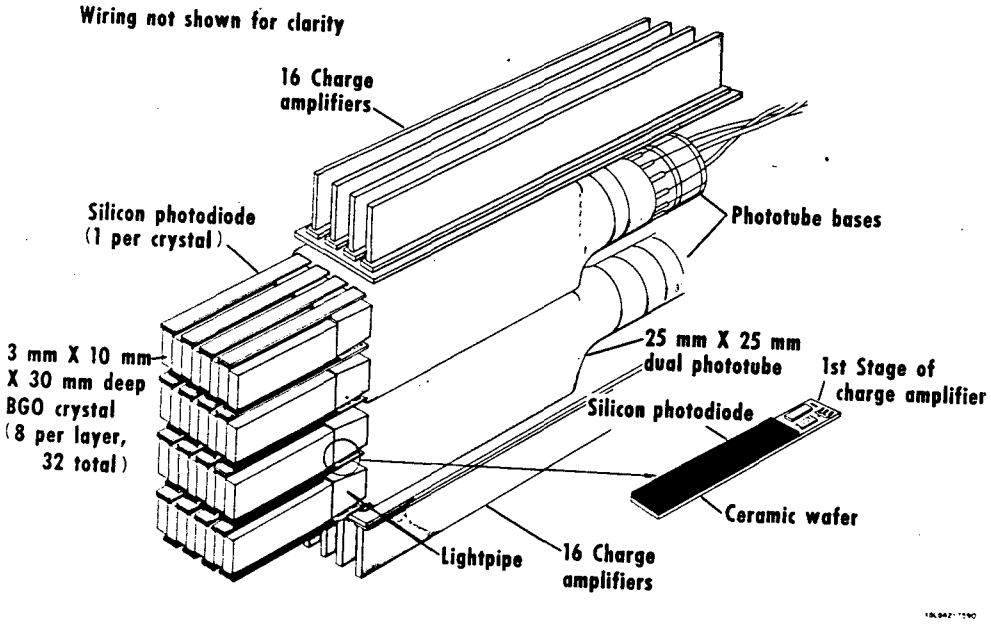

Figure 1: Multi-ring detector array where groups of 8 crystals are coupled to a common phototube for timing information and coupled individually to silicon photodiodes for the identification of the crystal of interaction. Square phototube (Hamamatsu R1548) has two independent electron multipliers and first stage of charge amplifier is mounted near photodiode.

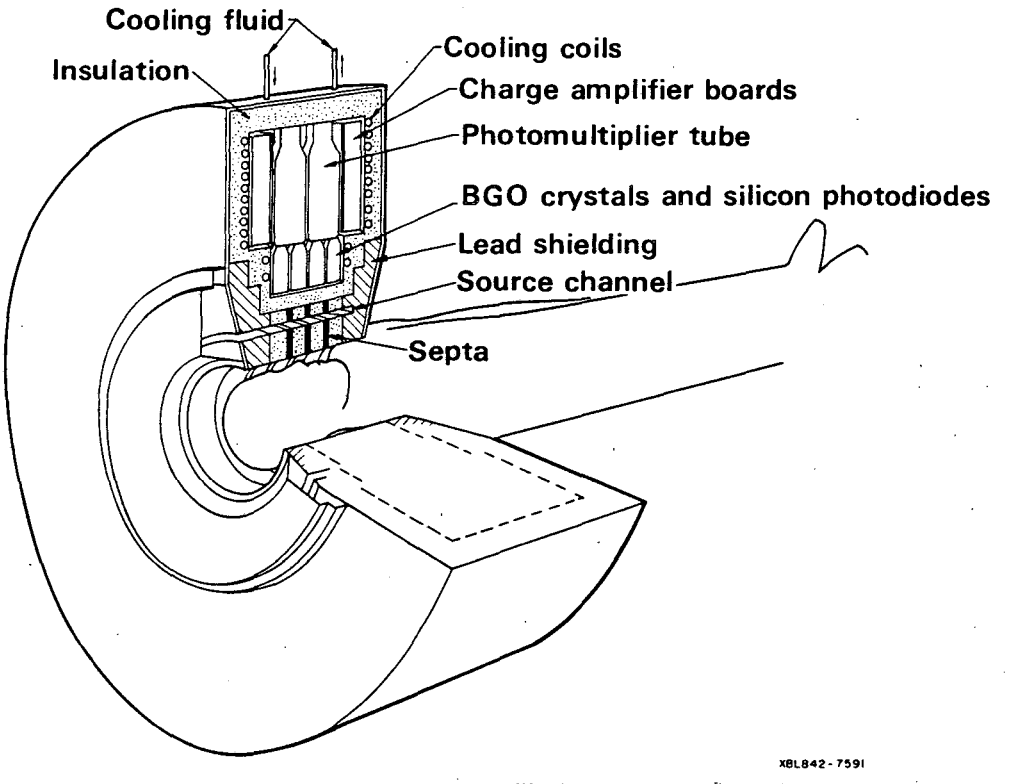

Figure 2: Cooled tomograph gantry for keeping silicon photodiodes and charge amplifiers at a reduced temperature (typically -30C°).

2 ULTIMATE LIMITS

To explore the ultimate limits of instrumentation in positron emission tomography, in the next section we introduce an ideal detector module, and then use it in the following sections to explore the ultimate spatial resolution, sensitivity, and maximum event rates.

2.1 A HIGH-RESOLUTION DETECTOR MODULE

Many recent high resolution detector systems rely on large numbers of small crystals for good spatial resolution (22-24). Although a spatial resolution of 2.5 mm fwhm has been achieved this way (22), a practical detector system with a spatial resolution finer than 1 mm may involve a smaller number of larger detectors that are able to measure the location of the recoil electron tracks from which all the scintillation photons originate. In the case of photoelectric absorption on the first interaction (which for 511 keV photons happens 44% of the time for BGO and 19% for BaF_2) all the light originates from a short (<1 mm long) recoil electron. In the case of multiple interactions (one or more Compton scatters followed by photoelectric absorption) the center of intensity of a pattern of recoil electron tracks would be measured.

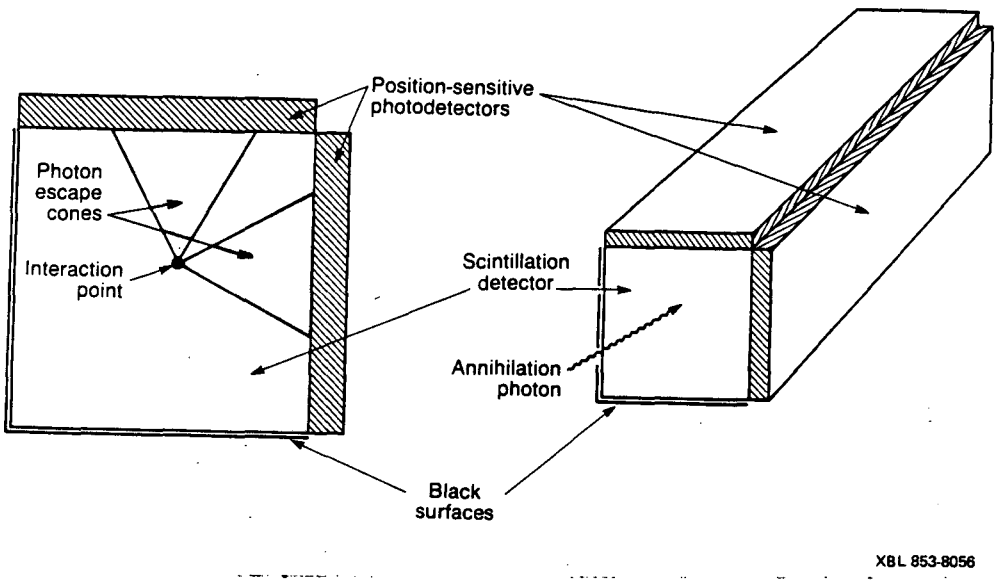

Figure 3: Detector module consisting of a rectangular scintillation crystal and photodetectors capable of determining the location of the interaction point within the crystal.

One scheme for this detector module is a scintillator block coupled to position-sensitive photodetectors on two orthogonal sides (Figure 3). The ideal photodetector for this application would be thin, have high quantum efficiency, be able to amplify photoelectrons internally with sufficient signal-to-noise that individual photons can be detected, and be able to determine position of the center of intensity of the arriving photons. Position sensitive silicon avalanche photodiodes or multi-anode phototubes may evolve to serve this function (20,25,26). The other sides of the crystal would be painted black so that any photon that does not reach a photodetector surface is absorbed. Photons reaching a photodetector surface outside an "escape cone" are internally reflected and absorbed on the other surfaces. Also, some photons within the escape cone are Fresnel reflected and absorbed. While this scheme collects only a small fraction of the available photons (see below), the collected fraction consists of photons that have spread the least in space and time. The opening angle θ_o for the escape cone is given by $sin(\theta_o) = n_2/n_1$, where n_1 is the index of refraction of the scintillator and n_2 is the index of refraction of the external window. For a heavy oxide crystal ($n_1 = 2$) and a glass window ($n_2 = 1.5$) between the scintillator and the photodetector, $\theta_o = 48.6°$. As determined by Monte Carlo calculation, 16% of the photons reach the photodetector (27).

Another potential candidate for this detector is a heavy element semiconductor with a 2-dimensional position sensitive readout (similar to the germanium gamma camera). If the electrons and holes have different drift velocity, the 3rd coordinate can be determined by measuring the pulse shape. Although subnanosecond timing has been achieved for germanium detectors (7,28), the detection efficiency and timing resolution of scintillators such as BaF_2 is significantly better, and we will restrict our considerations below to scintillation detectors.

If the ideal scintillation detector of table 1 and a thin, high-gain imaging photodetector were available, we could expect the following properties:

1) energy resolution: 8% fwhm, based on the statistical fluctuations of 1000 photoelectrons.

2) spatial resolution: less than 0.5 mm fwhm in x,y, and z, based on the fluctuations in the center of gravity of 1000 photoelectrons in an escape cone with a spread of 10 mm fwhm. If the interaction is close to the edge of the crystal, part of the escape cone is cut off, resulting in a non-linear response. It is expected that the correction factor can be measured and tabulated, and applied during data taking.

3) timing resolution: The number of photoelectrons and the decay time is similar to that of plastic detectors or BaF_2, which have achieved an annihilation pair coincidence timing resolution of 200 psec fwhm (4).

4) depth of interaction: By measuring the depth of interaction, the parallax error due to off-axis penetration can be essentially eliminated. In addition, the time-of-flight information can be corrected for the flight time of the scintillation photons in the crystal.

In the following sections we summarize the principal limits of PET instrumentation, given the scintillation detector module just described.

2.2 SPATIAL RESOLUTION

There are 7 primary contributions to spatial resolution in PET.

1) In positron emission, the positrons are emitted with a range of energies from zero to a maximum which varies from 640 keV for ^{18}F to 3350 keV for ^{82}Rb. Due to the non-linear relationship between energy and range for sub-relativistic charged particles (such as positrons below 200 keV), a significant fraction of the emitted positrons travel less than 1 mm in tissue. The resulting distribution has a central spike that preserves some of the high spatial frequency information and permits the deconvolution of the range broadening effects, but with some noise amplification (29).

2) Because the positron and electron are not at rest in the laboratory frame when they annihilate, they are not emitted at exactly 180° and have a Gaussian distribution with 0.5° fwhm (30). Unfortunately, such distributions are difficult to deconvolve because of the loss of information at the higher spatial frequencies. As a result, the random deviations from 180° emission is the most fundamental limit to spatial resolution in PET.

3) Detector Resolution, 4) Parallax error and 5) Sampling: By using a detector that can measure the location of the scintillation flash in 3-dimensions with good spatial resolution (< 1 mm fwhm), contributions from parallax error for off-axis rays, and limited linear sampling density are greatly reduced.

6) The high resolution imaging detector module mentioned above can only measure the center of energy deposition. In the case of a single photoelectric absorption interaction, the full energy is deposited in a small region along a short (<1 mm long) recoil electron track. In the case of one or more Compton scatters followed by photoelectric absorption the energy is deposited at several points several mm apart. Thus the distribution of measured positions consists of a sharp central spike flanked by tails that extend on each side by approximately one attenuation length (31,32). As with the positron range blurring, the multiple interaction blurring can be deconvolved with some amplification in statistical noise.

7) The motion of the head can be kept to within 1 mm during a $\leq$1 min imaging time in favorable cases. The motion of the heart is far greater and a blur of 2 mm is possible even when gating for both the beating of the heart and the motion of breathing.

TABLE 2. SUMMARY OF CONTRIBUTIONS TO SPATIAL RESOLUTION (fwhm)

FACTOR	HEAD[a]	HEART[b]
β^+ range	< 1 mm	< 1 mm
angulation error	1.3 mm	2 mm
detector resolution	< 1 mm	< 1 mm
off-axis penetration	< 1 mm	< 1 mm
sampling[c]	0 mm	0 mm
scatter in detectors	<1 mm	<1 mm
organ motion	<1 mm (fast scan)	2 mm (double gate)
TOTAL	2 mm	4 mm

[a]Detector ring diameter 60 cm
[b]Detector ring diameter 100 cm
[c]assuming continuous sampling

2.3 AXIAL RESOLUTION VS IN-PLANE RESOLUTION

Generally, different imaging planes are defined with trans-axial lead or tungsten shields and the design tradeoff between shielding gap and counting sensitivity results in an axial resolution that is 2 to 4 times coarser than the in-plane resolution. Using a detector module able to measure the point of interaction in all three spatial coordinates, the tomograph axial resolution could be as fine as the in-plane resolution. The proper utilization of the resulting out-of-plane rays will require a true 3-dimensional reconstruction algorithm able to use all the rays in an equatorial belt, resulting in a large number of image planes. For example, if the detector spatial resolution is 2 mm fwhm in all 3 dimensions and the volume to be imaged is 25 cm x 25 cm in the plane and 10 cm in axial thickness, then the reconstructed image set of 1 mm^3 pixels would consist of 100 transverse sections each consisting of a 256 x 256 array. Using a single video display, it is possible to view an image plane at any selected position, angular orientation, and thickness.

2.4 SENSITIVITY, SHIELDING APERTURE, AND SCATTER REJECTION

The greatest geometrical acceptance is achieved when the detector rings have greater axial extent than the organ to be imaged, and when the trans-axial shielding permits the detectors to record the full angular range of possible cross-plane coincidences. Two problems arise: 1) the geometrical acceptance of prompt scatter and random backgrounds (which are both non-collinear) is also large, and 2) reconstruction of data from a limited equatorial band is necessary. To address the first problem, we have used the methods of reference (33) to calculate the optimum shielding depth and determine the sensitivity and maximum event rates for a 10 cm shielding gap (Table 3). This wide shielding aperture provides an excellent imaging event rate but also introduces a large fraction of prompt scattered events. A pulse height resolution of 8% fwhm permits the rejection of pulses below 450 keV, but this corresponds to an in-plane angle cut-off of 30°, which has a limited ability to reject prompt scatters. Reducing the angle cut off to 5° would require a threshold of 509 keV, which is only possible using the best semiconductor detectors. The practical solution to this problem requires the accurate computation and subtraction of the prompt scatter background.

TABLE 3. POTENTIAL SENSITIVITY AND EVENT RATES

TOMOGRAPH PARAMETERS:	
Patient port diam P	30 cm
Shielding gap S	10 cm
Detection efficiency	70%
Coincidence window	3 nsec
Activity	1 μCi per cm^3 in a 20 cm cylinder of water
RESULTS OF SHIELDING DEPTH OPTIMIZATION	
Optimum shielding depth T	25 cm
Detector ring diameter (P+2T)	80 cm
Image event rate[a]	710,000 per sec
Random event rate[b]	550,000 per sec
Prompt scatter rate[c]	780,000 per sec
Total event rate	2,040,000 per sec
Effective event rate Q[d]	307,000 per sec

[a]Unscattered annihilation photon pair detected in coincidence. Only these events are collinear and can contribute to the image.
[b]Background due to unrelated photons detected in time coincidence by chance.
[c]Background due to annihilation photon pair detected in coincidence but one or both have scattered.
[d]Event rate needed in an ideal tomograph (no background events) for the same signal-to-noise ratio in the reconstructed image.

2.5 TIME-OF-FLIGHT

For a detector with a timing resolution that can localize the point of annihilation (along the line between the detector pairs) to a spatial accuracy (fwhm) of d, and for an emission distribution of effective diameter D, the time-of-flight information reduces the uncertainty in the reconstructed image and enhances the effective sensitivity by the factor D/d (34-38). The ideal time-of-flight scintillator would have a high single interaction photopeak efficiency (>60%), produce a large number of photons (>1000) in a short time (<1 nsec), and be able to measure the depth of interaction to compensate for the difference in velocity between the annihilation photon and the scintillation photons. The timing resolution should be better than 200 psec fwhm, which has been obtained with thin plastic scintillators (4). If D=18 cm (human head) and d=3 cm (200 psec), then D/d=6. This factor would increase the effective event rate described in the previous section to 1.8 x 10^6 non-time-of-flight events/sec for 1 μCi/cm^3. This sensitivity advantage is so large that the existence of the "ideal detector" would make time-of-flight a compelling consideration in all tomograph designs.

2.6 RANDOMS REJECTION AND MAXIMUM RATES

Even with arbitrarily good timing resolution, it is not possible to reject random events if their time-of-flight difference places them within the emission region. Thus the effective coincidence window for randoms acceptance is the electronic timing window or the size of the emission region, whichever is larger. For a quantitative analysis, see Ref. (39), where it is shown that in time-of-flight positron tomography, the statistical uncertainty in both the reconstructed true and random events is proportional to the detector timing resolution, and that the ratio is independent of the timing resolution. In table 3, we have used a coincidence window of 2 nsec, which corresponds to a 30 cm diam emission region. We see in this table that the randoms event rate is only slightly less than the image event rate, so 700,000 image events per sec represents a practical rate limit.

The maximum event rate is also a function of the detector deadtime and the number of detectors that are in the system. A large number of detectors operating in parallel permit a high maximum data rate. Electronics deadtime is not a fundamental limit, as many parallel circuits can be used.

3 CONCLUSIONS

The ultimate limits of PET instrumentation have not been realized because of the lack of: 1) an ultra-fast, high efficiency scintillator and 2) a thin photodetector with good timing and position accuracies. If these were available, then a multilayer time-of-flight tomograph would be possible with a 10 cm axial field of view, a 3-dimensional spatial resolution of 2 mm fwhm, and >700,000 prompt unscattered coincidences per sec for 1 μCi per cm^3 in a 20 cm diam cylinder of water.

ACKNOWLEDGEMENTS

I thank T. Budinger and R. Huesman for helpful discussions.

This work was supported in part by the Director, Office of Energy Research, Office of Health and Environmental Research of the U.S. Department of Energy, under Contract No. DE-AC03-76SF00098, and in part by the National Institutes of Health, National Heart, Lung, and Blood Institute under grant No. P01 HL25840.

Reference to a company or product name does not imply approval or recommendation of the product by the University of California or the U.S. Department of Energy to the exclusion of others that may be suitable.

REFERENCES

1. Farukhi MR and Swinehart CF: Barium fluoride as a gamma ray and charged particle detector. *IEEE Trans Nucl Sci* **NS-18(1):** 200-204, 1971
2. Weber MJ and Monchamp RR: Luminescence of $Bi_4Ge_3O_{12}$: spectral and decay properties. *J Appl Phys* **44:** 5495-5499, 1973
3. Gariod R, Allemand R, Cormoreche E, et al: The "LETI" positron tomograph architecture and time of flight improvements. *Workshop on Time-of-Flight Tomography,* IEEE Catalog No 82CH1719-3, 1982.
4. Laval M, Moszynski M, Allemand R, et al: Barium fluoride: inorganic scintillator for subnanosecond timing. *Nucl Instr Meth* 206: 169-176, 1983
5. Takagi K, and Fukazawa T: Cerium activated Gd_2SiO_5 single crystal scintillator. *Appl Phys Lett* **42:** 43-45, 1983
6. Kaufman L, Williams S, Hosier K, et al: An evaluation of semiconductor detectors for positron tomography. *IEEE Trans Nucl Sci* **NS-26:** 648, 1979
7. Kaufman L, Ewins J, Rowan W, et al: Semiconductor gamma cameras in nuclear medicine. *IEEE Trans Nucl Sci* **NS-27:** 1073-1079, 1980
8. Derenzo SE: Comparison of detector materials for time-of-flight positron tomography. *Proceedings of the International Workshop on Time-of-Flight Positron Tomography,* Thomas LJ and Ter-Pogossian MM, eds. pp 63-68, IEEE Computer Society Cat No 82CH1791-3, 1982.
9. Armantrout GA, Swierkowski SP, Sherohman JW, and Yee JH: What can be expected from high-Z semiconductor detectors? *IEEE Trans Nucl Sci* **NS-24:** 121-125, 1977
10. Ortendahl D, Kaufman L, Hosier K, et al: Operating characteristics of small position-sensitive mercuric iodide detectors. *IEEE Trans Nucl Sci* **NS-29:** 784-788, 1982
11. Barton JB, Hoffman EJ, Iwanczyk JS, et al: A high-resolution detection system for positron tomography. *IEEE Trans Nucl Sci* **NS-30:** 671-675, 1983
12. Groom DE: Silicon photodiode detection of bismuth germanate scintillation light, *Nucl Instr Meth,* **219:** 141-148, 1984
13. Iwanczyk JS, Barton JB, Dabrowski AJ, et al: A novel radiation detector consisting of an HgI_2 photodetector coupled to a scintillator. *IEEE Trans Nucl Sci* **NS-30:** 363-367, 1983
14. Derenzo SE: Initial characterization of a BGO-silicon photodiode detector for high resolution PET. *IEEE Trans Nucl Sci* **NS-31:** 620-626, 1984
15. Derenzo SE: Gamma-ray spectroscopy using small, cooled bismuth germanate scintillators and silicon photodiodes. *Nucl Instr Meth,* **219:** 117-122, 1984
16. Derenzo SE, Budinger TF, and Huesman RH: Detectors for high resolution dynamic PET. In *The Metabolism of the Human Brain Studied with Positron Emission Tomography,* T. Greitz and D. Ingvar, Eds, Raven Press, New York, pp 21-31, 1985

17. Entine E, Reiff G, Squillante M, et al: Scintillation detectors using large area silicon avalanche photodiodes. *IEEE Trans Nucl Sci* **NS-30:** 431-435, 1983

18. Lecomte R, Schmitt D, Lightstone AW, et al: Performance characteristics of BGO-silicon avalanche photodetectors for PET. *IEEE Trans Nucl Sci* **NS-32:** 482-486, 1985

19. Dahlbom M, Mandelkern MA, Hoffman EJ, et al: Hybrid mercuric iodide (HgI_2) – gadolinium orthosilicate (GSO) detector for PET. *IEEE Trans Nucl Sci* **NS-32:** 533-537, 1985

20. Squillante MR, Reiff G, and Entine G: Recent advances in large area avalanche photodiodes. *IEEE Trans Nucl Sci* **NS-32:** 563-566

21. Yamashita Y, Uchida H, Yamashita T and Hayashi T: Recent development in detectors for high spatial resolution positron CT. *IEEE Trans Nucl Sci* **NS-31:** 424- 428, 1984

22. Derenzo SE, Huesman RH, Budinger FT, Cahoon JL, and Vuletich T: High resolution positron emission tomography using 3 mm wide bismuth germanate crystals, 1985 (in preparation)

23. Computer Technology and Imaging, Inc. Knoxville, Tennessee, MODEL PT 931 ECAT Scanner System Description.

24. Burnham CA, Bradshaw J, Kaufman D, et al: Design of cylindrical shaped scintillation camera for positron tomographs. *IEEE Trans Nucl Sci* **NS-32:** 889-893, 1985

25. Timothy JG: Electronic readout systems for microchannel plates. *IEEE Trans Nucl Sci* **NS-32:** 427-432, 1985

26. Kume H, Suzuki S, Takeuchi J, et al: Newly developed photomultiplier tubes with position sensitivity capability. *IEEE Trans Nucl Sci* **NS-32:** 448-452, 1985

27. Derenzo SE and Riles J: Monte Carlo calculations of the optical coupling between bismuth germanate crystals and photomultiplier tubes. *IEEE Trans Nucl Sci* **NS-29:** 191-195, 1982

28. Bengtson B and Moszynski M: Subnanosecond timing with planar Ge(Li) detectors. *Nucl Instr Meth* **100:** 293, 1972

29. Derenzo SE: Mathematical removal of positron range blurring in high resolution tomography, 1986 (in preparation).

30. Colombino P, Fiscella B, Trossi L: Study of positronium in water and ice from 22 to -144 °C by annihilation quantum measurements. *Nuovo Cimento* **38:** 707-723, 1965

31. Anger HO: Survey of radioisotope cameras. *ISA Trans* **5:** 311-334, 1966

32. Parker RP: Degradation of spatial resolution in gamma cameras employing sodium iodide or germanium detectors. *Phys Med Biol* **15:** 493-502, 1970

33. Derenzo SE: Method for optimizing side shielding in positron emission tomographs and for comparing detector materials. *J Nucl Med* **21:** 971-977, 1980

34. Budinger TF, Derenzo SE, Greenberg WL, Gullberg GT, and Huesman RH: Quantitative potentials of dynamic emission computed tomography. *J Nucl Med* **19:** 309-315, 1978

35. Allemand R, Gresset C, and Vacher J: Potential advantages of a Cesium Fluoride scintillator for a time-of-flight positron camera. *J Nucl Med* **21:** 153-155, 1980

36. Snyder DL, Thomas LJ and Ter-Pogossian MM: A mathematical model for positron-emission tomography systems having time-of-flight measurements. *IEEE Trans Nucl Sci* **NS-28:** 3575-3583, 1981

37. Snyder DL: Some noise comparisons of data-collection arrays for emission tomography-systems having time-of-flight measurements. *IEEE Trans Nucl Sci* **NS-29:** 1029-1033, 1982

38. Tomitani T and Tanaka E: Image reconstruction and noise evaluation in photon time-of-flight assisted positron emission tomography. *IEEE Trans Nucl Sci* **NS-28:** 4582-4589, 1981

39. Holmes TJ, Ficke DC, and Snyder DL: Modeling of accidental coincidences in both conventional and time-of-flight positron-emission tomography. *IEEE Trans Nucl Sci* **NS-31:** 627-631, 1984

This report was done with support from the Department of Energy. Any conclusions or opinions expressed in this report represent solely those of the author(s) and not necessarily those of The Regents of the University of California, the Lawrence Berkeley Laboratory or the Department of Energy.

Reference to a company or product name does not imply approval or recommendation of the product by the University of California or the U.S. Department of Energy to the exclusion of others that may be suitable.

TECHNICAL INFORMATION DEPARTMENT
LAWRENCE BERKELEY LABORATORY
UNIVERSITY OF CALIFORNIA
BERKELEY, CALIFORNIA 94720